

Flow-based network analysis of the *Caenorhabditis elegans* connectome

Karol A. Bacik,^{1,*} Michael T. Schaub,^{2,3,†} Mariano Beguerisse-Díaz,¹ Yazan N. Billeh,⁴ and Mauricio Barahona^{1,‡}

¹*Department of Mathematics, Imperial College London, London SW7 2AZ, United Kingdom*

²*naXys & Department of Mathematics, University of Namur, B-5000 Namur, Belgium*

³*ICTEAM, Université catholique de Louvain, B-1348 Louvain-la-Neuve, Belgium*

⁴*Computation and Neural Systems Program, California Institute of Technology, CA 91125 Pasadena, USA*

(Dated: September 6, 2022)

We present a flow-based network analysis of the directed connectome of the nematode *C. elegans*. Unlike other network analysis tools, which are mainly based on structural or topological graph properties, our framework adopts a dynamical viewpoint, using directed flow propagation on the graph as a means to revealing relevant features of the network. First, we use Directed Markov Stability community detection to find flow-retaining groupings of neurons at different levels of granularity, which are then related to functional and anatomical features. We then carry out a systematic *in silico* evaluation of the full set of single and double ablations in the network, in order to identify node deletions that induce the most severe disruptions to the multi-resolution community structure. Such ablations are shown to be linked to functionally relevant neurons and suggest potential candidates for further *in vivo* investigation. Second, we use the Role Based Similarity framework to identify four flow roles for the neurons in the connectome, based on the pattern of incoming and outgoing network flows for each node and without pre-imposing an *a priori* classification. The flow roles identified are related to neuronal classifications and functionally important neuronal circuits, and interpreted in the light of signal propagation from biologically motivated inputs.

I. INTRODUCTION

The nematode *Caenorhabditis elegans* has been used as a model organism in the life sciences for almost half a century [1]. A considerable amount of effort has been devoted to elucidating the properties of its nervous system in relation to functional behaviour. The *C. elegans* connectome was originally charted in 1986 by White et al. [2] and has been refined by further analysis and experiments [3], most recently in the work of Varshney et. al [4]. Furthermore, using experimental techniques such as laser ablations, calcium imaging, optogenetics and sonogenetics, researchers have examined functional properties of individual neurons in connection with motion, learning, or information processing and integration [5–9]. There are also some promising studies quantifying the motion of *C. elegans*, and how it changes upon genetic mutations [10–12].

With the increased availability of such experimental techniques, there is a need to integrate current knowledge of individual neurons into a comprehensive picture of how the network operates systemically [2, 4, 13]. A number of studies have investigated network characteristics of the *C. elegans* connectome: it is a small-world network [14] with a heavy-tailed degree distribution [15] and a core-set of highly-connected ‘rich club’ neurons [16] satisfying some mathematical efficiency criteria [17]. Analyses of the modular structure of the connectome showed that it is often possible to match strongly-coupled clusters of neurons to circuits involved in a variety of biolog-

ical functions [18–22]. These observations suggest that a system-wide analysis of the connectome can provide valuable functional information. However, finding simplified mesoscale descriptions that can coherently aggregate how information propagates in the directed connectome across multiple scales remains a challenge.

In this paper, rather than focusing on purely structural features of the network, we analyse the directed, weighted graph of the *C. elegans* connectome from a flow-based perspective. Our methodology uses diffusive processes on graphs as a simple means to study the link between network structure and directed propagation dynamics. Firstly, we investigate the presence of flow-based partitions of the connectome across multiple scales using the Markov Stability (MS) framework for community detection [23–25]. Our analysis detects subgroups of neurons that retain diffusive flows over particular time scales [26], taking into account edge directionality [25, 27]. Secondly, we provide an alternative analysis of directed flows through the Role Based Similarity (RBS) framework [28–30]. RBS classifies neurons into *flow roles*, which are directly extracted from the network based on the (asymmetric) patterns of incoming and outgoing flows (at all scales), without pre-imposing characteristics for the types. The MS groupings and RBS roles are linked to functional properties of the neurons.

While diffusive flow propagation is a raw simplification of the actual dynamical behaviour of the nervous system of *C. elegans*, it can provide us with a first insight into network features of dynamical interest, as discussed by Varshney and coworkers in Ref. [4]. Through this simplified dynamics, we can also mimic wet-lab experiments and compare the *in silico* results with the corresponding real-world observations. In particular, we conduct two types of computational experiments. Firstly,

* karol.bacik13@imperial.ac.uk

† michael.schaub@unamur.be

‡ m.barahona@imperial.ac.uk

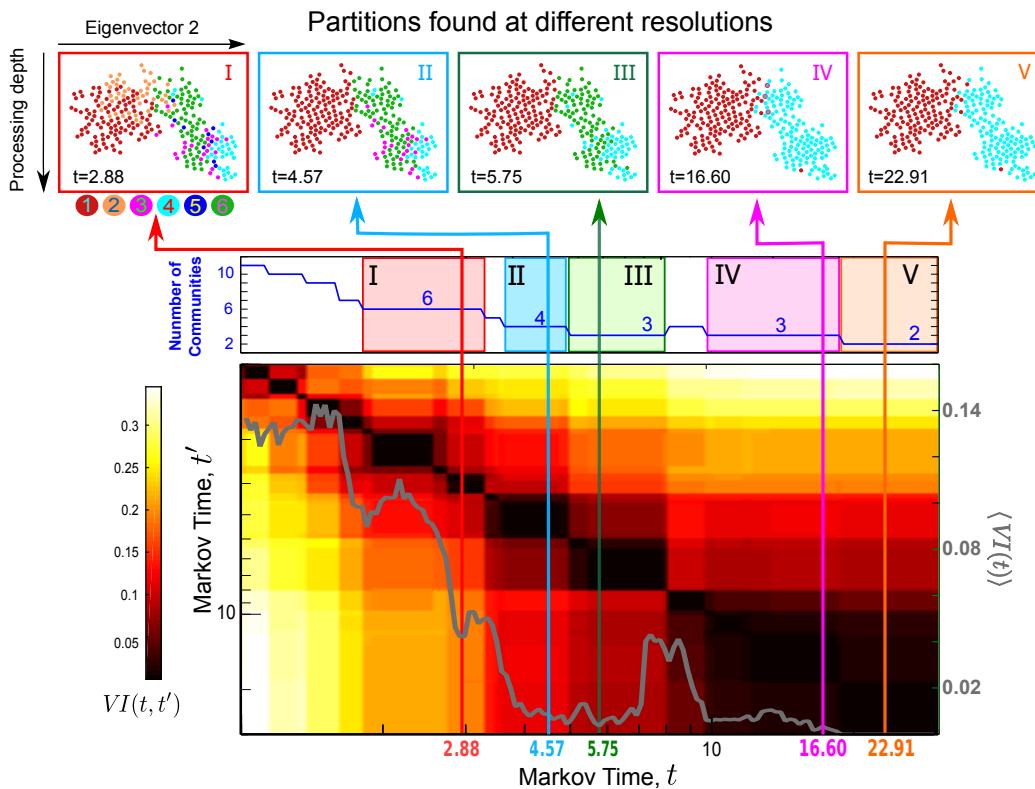


Figure 1. **Flow-based multiscale partitioning of the connectome of *C. elegans*.** Using Markov Stability, we detect flow-based partitions in the *C. elegans* connectome at all scales (see Fig. S1 in the *SI* for the full sweep of Markov time). Here we present the medium to coarse Partitions I to V (top panel), which are found as optimal at each of the indicated Markov time intervals. Partitions I-V are persistent across time, as shown by the extended plateaux in $VI(t, t')$, and robust with respect to the optimisation, as measured by decreased variation of information $\langle VI(t) \rangle$ (lower panel; see Methods section).

we mimic neuronal ablations within our computational framework. We check *all* possible single and double ablations in the connectome and detect the most disruptive of the flow-based modular organisation found using MS. Secondly, we mimic a ‘stimulus-response’ experiment [8, 9], in which we excite well-defined sets of sensory neurons corresponding to biological stimuli, and we observe the time course of signal propagation in the network. Through the observed dynamics, we relate the flow roles found with RBS to features of information processing in the nervous system of *C. elegans*. Our *in silico* explorations are consistent with experimental findings, suggesting that our framework can provide guidance towards the identification of potential neuronal targets for further *in vivo* experiments.

II. RESULTS

Our analysis of the *C. elegans* connectome is based on the data reported in Ref. [4] (see www.wormatlas.org/neuronalwiring.html). We study the weakly connected giant component of this network, which contains 279 neurons with 6394 chemical synapses (directed) and 887 gap junctions (bidirectional). Ref. [4] also provides the po-

sition of the soma of each neuron along the body of the worm, and classifies each neuron as either sensory (S), interneuron (I) or motor (M).

A. Flow-based partitioning reveals multi-scale organisation of the connectome

We use the Directed Markov Stability (MS) framework as described in Sec. IV C to reveal the multi-scale organization of this network. Conceptually, Markov Stability can be understood as follows. Imagine a drop of ink (signal) is placed on a node and starts diffusing. If the graph does not have any modular structure, the ink will diffuse isotropically and its concentration will rapidly reach the stationary solution. However, if the graph does have a modular structure the flow will be trapped in certain subgraphs for longer than expected, indicating that particular sets of nodes are strongly coupled to each other and more weakly connected to the rest of the network; in other words, those nodes form *communities*. If we observe the ink diffusing for a short interval of time, only small communities are detected, since the ink does not have time to explore the whole extent of the network. If we observe the process for a longer time, the diffusion

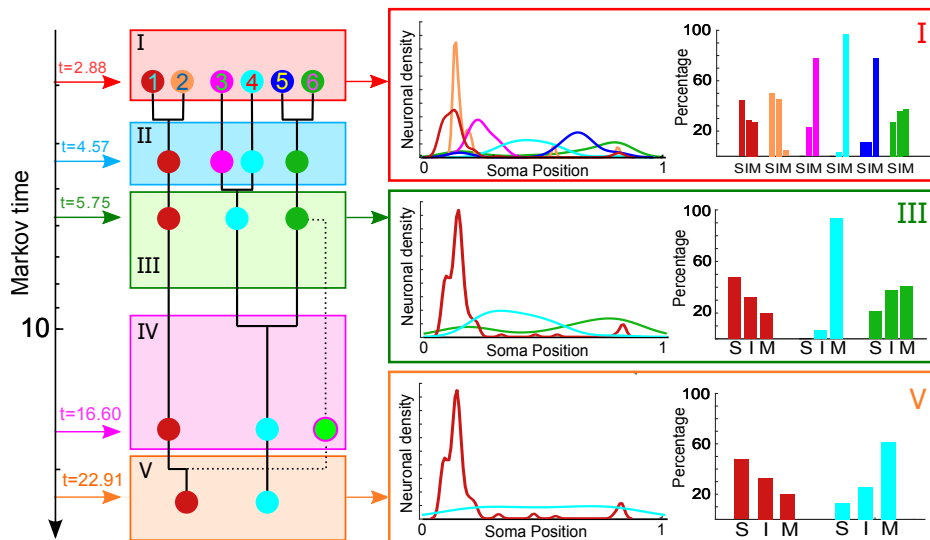


Figure 2. **Community structure and biological features.** Left: As indicated by the non-binary dendrogram, the partitions obtained have a quasi-hierarchical organisation. Middle: Smoothed densities of neurons in each community for different partitions. Note that the communities are largely separated according to the soma positions of the neurons. The merging of groups over Markov time largely retains this spatial structure. Right: Percentages of sensory (S), inter- (I) and motor (M) neurons in each community showing the functional segregation in particular groupings.

explores larger parts of the network and the communities detected can be larger. In this sense, the time of the diffusion process, denoted by *Markov time* in the following, acts as a resolution parameter. By scanning across all Markov times, we are able to extract cohesive node groupings at different levels of granularity [25, 26, 31].

Figure 1 shows the community structure of the *C. elegans* connectome at medium to coarse levels of resolution. The full scan across all Markov times is shown in Figure S1 of the SI, and the full set of optimal partitions at all Markov times can be found in the Supplementary Data 1. As described above, the partitions become coarser as the Markov time t increases, from very fine partitions to the dominant bipartition at long times. Our analysis focuses on the late Markov times (Fig. 1), where there are robust partitions containing 6 to 2 communities. As shown in Fig. 2, the partitions exhibit an almost hierarchical structure as we go towards coarser descriptions, with a strong spatial localisation and a relation to functional and organisational circuits. In the Supplementary Material, we provide spreadsheets with the neurons in each of the communities and all the features discussed. We now expand briefly on some of the characteristics of the partitions found.

Medium resolution (Partitions I to III): The robust Partition I ($t = 2.98$; red frame in Fig. 1) comprises six communities of varying sizes (from 9 to 104 neurons), which are well localised along the body of the worm, as seen in Fig. 2 (c.f. also Section 2.2 in www.wormatlas.org/neuronalwiring.html). The partition has two large communities of head ganglia neurons (C1 and C2) which contain neurons of all three functional

types (S, I, M): C1 contains a variety of ring motor neurons and interneurons as well as the posterior neurons ALN and PLN; C2 specifically gathers amphid neurons, such as AWAL/R, ASKL/R, ASIL/R, AIYL/R, which feature prominently in the navigation circuit responsible for exploratory behaviour [32]. The next communities (C3, C4, C5) in Partition I consist predominantly of ventral cord motor neurons, yet they are differentiated by their soma position along the body (Fig. 2): C3 contains frontal motor neurons (VD1-3); C4 consists of mid-body motor neurons (VD4-8); and the small community C5 contains posterior motor neurons (VD9-10). This particular division provides further evidence for the motor neurons segmentation model which has been proposed for *C. elegans* [33]. Finally, C6 contains highly central neurons such as AVAL/R or PVCL/R, which have been found to belong to a *rich-club* [16], as well as many interneurons in charge of mechanosensation and the tap withdrawal functional circuits [20].

Partitions II and III correspond to quasi-hierarchical agglomerations of Partition I (see Figs. 2 and 2). Partition III has groupings of head ganglia (red, merged C1 and C2); frontal motor neurons (cyan, merged C3 and C4); and a tail group (green, merged C5 and C6). It is important to remark that our community detection method does not enforce a hierarchical agglomeration of communities (see Partition IV below as a contrasting example). Hence the observed quasi-hierarchy is an intrinsic feature of the connectome.

Coarse resolution (Partitions IV and V): Partition IV is a distinct, coarser 3-community partition, which is robust and optimal at later Markov times. Note

how this partition exemplifies how our method does not enforce a strict hierarchy in the multiscale structure. Partition IV has 3 groups, including a notable community of only three nodes (interneurons AVFL/R and AVHR), which appear as a strongly cohesive group only at this particular timescale. The prominent functional role of the AVF and AVH neurons has been noted previously [4, 34]: both AVF neurons are reportedly responsible for coordination of egg-laying and locomotion [35]. In addition, spectral analyses of the gap-junction network Laplacian have shown that AVF, AVH, PHB and C-type motor neurons are strongly coupled [4]. The two other communities in Partition IV correspond largely to those in Partition V.

The two groups in the final partition (Partition V) split the connectome anatomically into one group with head and tail ganglia, and another group predominantly composed of motor neurons.

B. The effect of single and double ablations on flow-based communities

Laser ablation experiments are invaluable to understand the functional role of neurons [5–7, 36], but are time-consuming and technically challenging. Here, we use our computational framework to assess the effect that single and double ablations have on network flow distribution by measuring the disruption they induce in the MS partitions obtained above. If an ablation induces strong distortions in the flows of the network, the partitions in the ablated network will change drastically or become less robust as compared to those found in the original, unablated network. We have carried out a systematic computational analysis of the effect of *all* single and double ablations in the network.

1. Single neuron ablations: disrupting the partitions and altering their robustness

Ablations that disrupt the robustness of the partitions: In some cases, the ablation of a neuron can have a strong effect on the robustness of specific partitions. To detect such ablations, we compute a Gaussian Process Regression (GPR) to describe the $\langle VI(t) \rangle$ of the ensemble of *all* single node ablations (Fig. 3a), and obtain the single ablations that appear as sustained outliers over Markov time for each of the Partitions I–V (Fig. 3b). For more details, see Section IV D in Methods.

Only seven ablations satisfy our criterion for a major disruption (see Section IV D) of any of the Partitions I–V. Three single ablations have a major effect on the robustness of Partition I. The ablations of the interneuron PVCr and of the motor neuron DD3 both decrease the robustness of Partition I. PVCr (C6) and DD3 (C4) play the role of internal authorities for their communities, with many incoming connections, and both of these

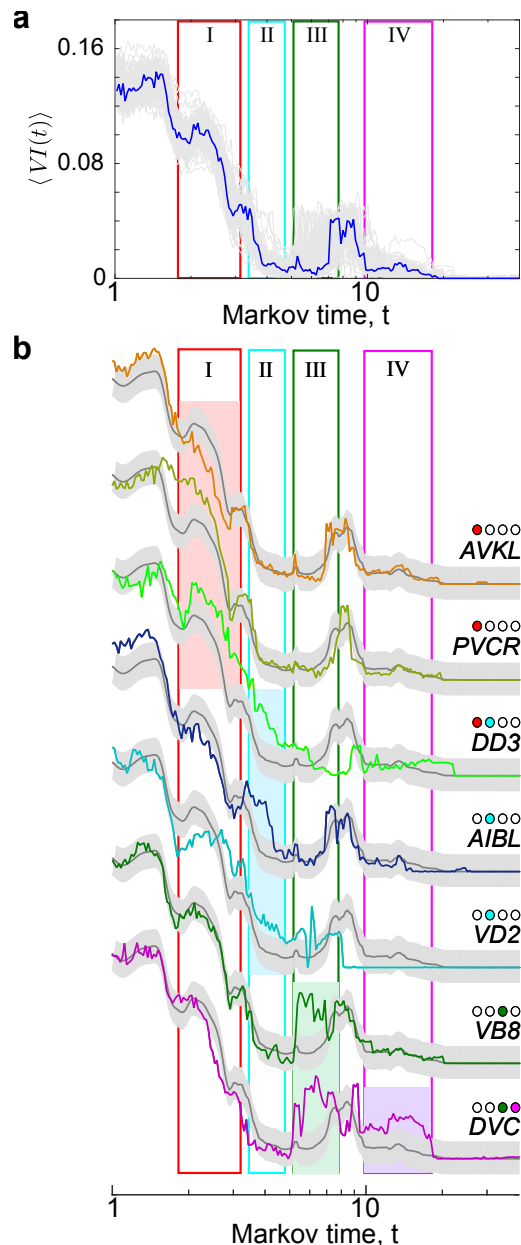


Figure 3. **Single partitions inducing loss of robustness of particular partitions.** (a) Ensemble of $\langle VI(t) \rangle$ profiles of *all* single node ablations (light gray lines) and the intact connectome (blue). (b) A Gaussian process (GP) is fitted to the ensemble of single node ablations in (a). The GP is described by the mean $\mu(t)$ (thicker dark grey line) and standard deviation (grey bands). Sustained outliers from this GP are identified using a statistical criterion (see Methods). Seven outliers are found affecting different partitions, as indicated by the coloured dots.

neurons are critical at different stages of motor action: PVCr drives motion whereas DD3 coordinates it. The third important ablation is that of interneuron AVKL, which links community C1 (head) with community C3 (ventral cord) and community C6 (rich club). The in-

creased robustness of the community structure upon ablation of AVKL indicates a decreased communication between these groups. As the function of AVKL is uncharted at present [37], one may only speculate about behavioural changes that can only be verified experimentally. For Partition II, there are also three important ablations. The ablations of DD3 (again) and of VD2, which is also a D-type motor neuron only on the ventral side, are both disruptive of Partition II. In addition, the ablation of the amphid interneuron AIBL also appears as relevant. AIBL is a bridge between C1 and C2, which merge in Partition II (see Fig. 2). The prominent role of amphid interneurons will become apparent when considering double ablations, as seen in the next section. Partition III is rendered non-robust by the ablation of VB8 (motor neuron responsible for forward locomotion) and by the ablation of interneuron DVC. Both VB8 and DVC are in C5 and DVC has links with all C3-C6, hence its ablation affects the subsequent merging of these groups. Indeed, the ablation of DVC reduces the robustness of both 3-way partitions (III and IV), thus blurring the multiscale organisation of the spatial segments of motor neurons. This indicates that DVC might integrate feedback from different parts of the body, in accordance with recent studies suggesting that DVC may act as a stretch receptor [38].

Ablations that induce large changes in the make-up of the optimal partitions: To measure how much each partition is affected by any of the single-ablations, we use the community variation, CV , defined in Eq. (12) in the Methods section. A high value of $CV_{[i]}(\mathcal{P})$ indicates a large disruption in the make-up of partition \mathcal{P} under the single ablation of neuron i .

Table I. Neurons with top five Community Variation ($CV_{[i]}(\hat{\mathcal{P}}(t))$) for each Partition I-V. The neuron type is indicated in parenthesis (M: Motor; I: Interneuron; S: Sensory).

Partition				
I	II	III	IV	V
DD3 (M)	DD3 (M)	DD2 (M)	DD2 (M)	DD2 (M)
SMDDR (M)	DD4 (M)	AVAL (I)	AVAR (I)	AVAR (I)
DD4 (M)	VD2 (M)	AVAR (I)	RMDVL (M)	RMDVL (M)
VD1 (M)	DD2 (M)	DD3 (M)	RIAR (I)	RMDDR (M)
DD2 (M)	VD6 (M)	DD5 (M)	RIAL (I)	AVER (I)

Our analysis of CV shows that the ablation of some neurons can be completely destructive of Partitions I and II. In particular, the ablations of DD3 or SMDDR induce severe changes in the network structure so that a partition similar to I is no longer found at any Markov time, indicating that the flow organisation has been drastically altered. For the finer Partitions I and II, ablations of D-type motor neurons coordinating motion (e.g., DD2, DD3, VD1, VD2) have particularly severe effects. It is interesting to note that D-type motor neurons have significantly higher PageRank (median 0.0092, compared to overall median of 0.0018; two-sided Wilcoxon rank test $p = 2 \times 10^{-7}$), and their synapses appear as critically

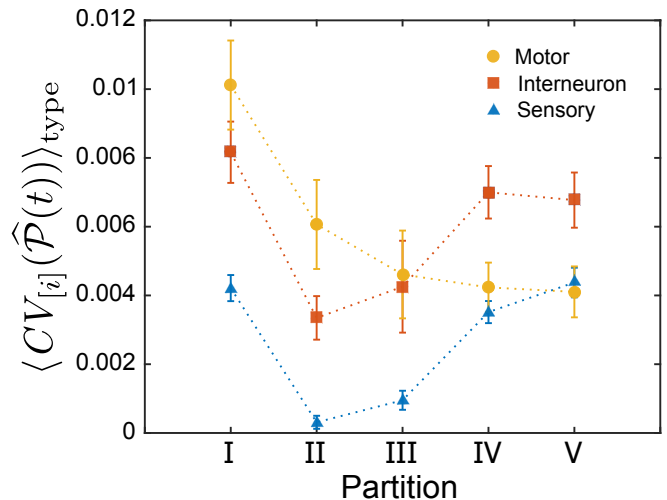


Figure 4. **Effect of single ablations on different partitions by neuron type.** We compute the community variation $CV_{[i]}(\hat{\mathcal{P}}(t))$, as defined in Eq. (12), for Partitions I-V and we average it over all single ablations of each type: sensory (blue), inter- (red) and motor neurons (yellow).

embedded edges with few alternative routes in other network analyses [34].

We find that the ablation of command neurons, such as AVAL/R and AVER, as well as second layer interneurons RIAL/R and ring motor neurons RMD have important effects on the coarser Partitions III-V. These are highly central neurons and our method confirms that their deletion introduces heavy distortions on the global flow of the connectome.

In Table I we show the five neurons with highest CV with respect to each of the Partitions I-V. Interestingly, none of them is a sensory neuron—all of them are motor or inter-neurons. This indicates that although the ablation of sensory neurons can have strong local effects (e.g., the inability to detect a particular stimulus) their ablation is not significant for global information flow.

Further confirmation of the importance of I and M neurons is given in Figure 4, where we show the average CV of a single ablation in the Sensory, Interneuron and Motor groups. On average, motor neurons have a larger effect on the local level structures reflected in the finer Partitions I and II, whereas interneurons induce larger changes in the coarser Partitions IV and V related to global flows.

2. Double neuron ablations: beyond additive effects

We have also performed an exhaustive *in silico* exploration of all possible 38781 combinations of two-neuron ablations. Specifically, we look for pairs of neurons whose simultaneous ablation is more disruptive than one would expect from the additive effect of the corresponding two single ablations. To achieve this, we compute the Com-

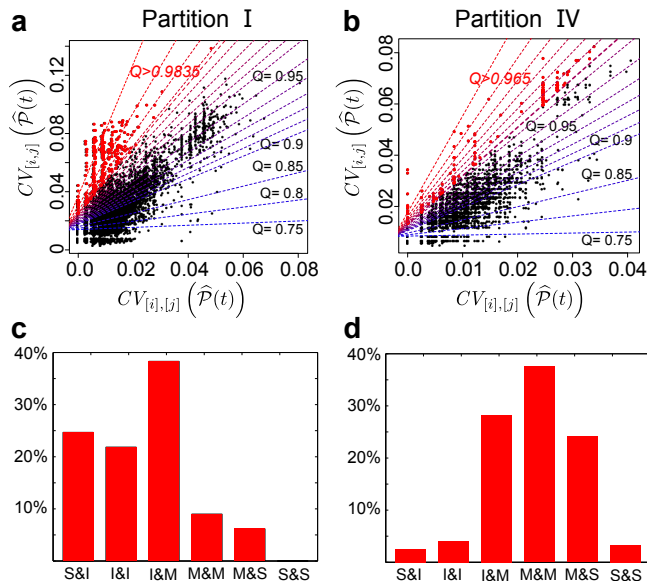


Figure 5. **Detecting double ablations with supra-additive effects.** Using Quantile Regression, we all two-neuron ablations in the network by comparing the additive effect of the two single ablations against the combined effect of the double ablation. We compute the CV of the pair and the sum of the two ablations (see Section IV D 2) and we select the top 1% outlying two-node ablations for Partition I (a) and Partition IV (b). (c) The top 1% double ablations disrupting Partition I are dominated by interneurons, whereas (d) the top 1% of double ablations disrupting Partition IV are dominated by motor neurons.

munity Variation for each possible double ablation, and compare it to the summed CV of the corresponding single ablations. We then use quantile regression to identify the double ablations that have a large combined effect beyond the merely additive. For more details, see Section IV D 2 in Methods.

As for the single ablations, different double ablations can perturb the community structure at different levels of granularity. Here we focus on disruptions to Partitions I and IV, which represent prototypically the partitions at medium and coarse granularity, respectively. The results of our quantile regression are shown in Figure 5a-b, where we also indicate the top 1% ablations according to their supra-additive effect for Partitions I and IV (above quantiles 0.9835 and 0.965, respectively).

As the word clouds in Fig. 5 show, double ablations containing neuron AIAR and DD2 have exceptionally often supra-additive effects for Partitions I and IV, respectively. Interestingly, 85% of the top supra-additive double ablations for Partition I contain at least one interneuron, whereas 90% of the top supra-additive double ablations for Partition IV contain at least one motor neuron (see Fig. 5c-d). This observation complements the results for single ablations in Figure 4, where interneurons are shown to be more substantially disruptive for Partition IV, and motor neurons for Partition I.

Considering both partitions at once, very few double ablations introduce large supra-additive effects for both the medium and large scales: the nine double ablations that appear in the top 1% for both the finer (Partition I) and coarse (Partition IV) resolutions are presented in Table II. Interestingly, eight of these nine pairs contain interneuron AIAR. The amphid interneurons AIA (along with AIB, AIY and AIZ) have a specific position in the connectome: they receive synapses from sensory neurons driving motion. Their prominent role in locomotion integration has been previously discussed and backed by *in vivo* ablation experiments [6]. Our results indicate that the deletion of pairs of neurons involving AIAR would have a magnifying effect on the disruption of the flow-based organisation at all scales of the connectome.

Table II. Double neuron ablations which lead to supra-additive disruption for both Partitions I and IV (within the top 1% in both partitions according to Quantile Regression).

Neuron pair	Types
AIAR + AQR	I & S
AIAR + AVEL	I & I
AIAR + DA2	I & M
AIAR + VA2	I & M
AIAR + VB2	I & M
AIAR + VD5	I & M
AIAR + VD6	I & M
AIAR + PVCR	I & I
AQR + SAAVL	S & I

C. Identifying flow roles in the directed connectome: functional relevance

A complementary analysis of the directed connectome of *C. elegans* is provided by the Role Based Similarity (RBS) framework [28, 29]. RBS identifies *flow roles* for the nodes of the network without imposing node types or number of types *a priori* by a direct evaluation of the patterns of incoming and outgoing flows given by paths of all lengths. Because they include information at all scales, the flow roles so obtained can extract more detailed information about the particular network, as compared to standard pre-defined classifications into, e.g., sources, sinks and hubs. Importantly, our flow roles also reveal subtle features beyond those derived from immediate neighbourhoods (e.g., notions of social roles based on Structural Equivalence [39] and Regular Equivalence [40]). Details of the RBS methodology are given in Refs. [27, 28, 30], and summarised briefly in Sec. IV E and in the *SI* (Figs. S2 and S3).

The RBS analysis extracts four distinct *flow roles* for the neurons in the *C. elegans* connectome (Fig. 6a; see

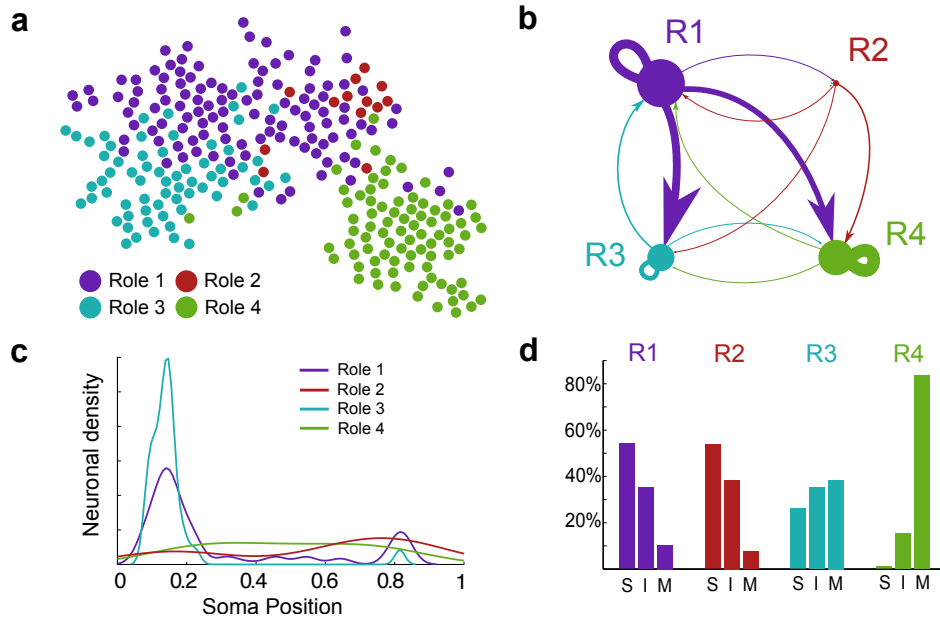


Figure 6. **Flow roles for neurons in the *C. elegans* connectome.** (a) Using the Role Based Similarity (RBS) framework (see Fig. S2 in *SI*), we detect four relevant flow roles in the connectome. (b) The coarse-grained representation indicates the flow profiles of the roles: there are two upstream roles (R1, R2), with a dominant source character, and two downstream roles (R3, R4), with a dominant sink character. Yet each role has distinctive in- and out- flow patterns. (c) Spatial density of neurons for each role: R1 and R3 are localised predominantly in the head, whereas R2 and R4 are spread along the body. Note how the upstream role R2 has significant localisation in the tail. (d) Proportions of sensory (S), inter- (I) and motor neurons (M) in each role.

Supplementary Data 2 for details). Two of the roles obtained (R1 and R2) have a dominant ‘source’ character (i.e., higher average in-degree than average out-degree); conversely, the other two roles (R3 and R4) have a dominant ‘sink’ character. As seen in Fig. S2 of the *SI*, R1 and R2 concentrate most of the nodes with high PageRank, whereas R3 and R4 are mostly formed by nodes with low PageRank. Yet, as seen in Fig. 6bc, these four roles are not only distinguished by such average properties but also by their global flow patterns: R1 is upstream from roles 3 and 4, whereas R2 is upstream only from R4. Additionally, R4 is an almost pure downstream module, whereas R3 has a stronger feedback connection with R1.

These flow roles are linked to biological features of the neurons. R4 corresponds to a group of motor neurons (mostly ventral chord motor neurons) consistent with its downstream character. R1 is a group of mostly sensory and inter-neurons with heavy localisation in the head. R3 is a group with a balanced representation of all three types of neurons (including a few polymodal neurons) localised in the head ganglion. In fact, the large majority of ring neurons in R3 are also in community C1, indicating that the head ganglion neurons form a self-contained unit that process head specific behaviour such as foraging movements and head withdrawal reflex [37]. Perhaps most interestingly, RBS reveals a specific role (R2) for a small group of neurons, with a heavy over-representation of sensory and interneuron types lying upstream mainly

from the motor neurons in R4. R2 contains thirteen neurons, the majority of which are responsible for escape reflexes triggered in the presence of a noxious factor (see Tabls III). Hence we term the R2 group as *escape response neurons*. The R2 neurons include: the PVDL/R neurons, which sense cold temperatures and harsh touch along the body; FLPL/R, which perform the equivalent task for the anterior body region; PHB neurons responsible for chemorepulsion; PHCR, which detects noxiously high temperatures in the tail; SDQL and PQR, which mediate high oxygen and CO₂ avoidance, respectively; and PLMR, a touch mechanosensor in the tail [2]. This escape response group is also heavily over-connected to command neurons AVAL/R, AVDL/R, DVA, PVCL/R, all of which modulate the locomotion of the worm. Specifically, there are 48 connections from the R2 escape response group to these particular command neurons, in stark contrast to the ~ 12 connections that would be expected at random. Note that neurons AVDL/R and DVA are in R1, whereas AVAL/R and PVCL/R are in R4; hence the R2 group links directly to motor locomotion neurons across the worm. We remark that this group of neurons was found exclusively through the analysis of their in/out connectivity profiles, without any other external information.

Table III. **Role 2 (R2) neurons:** These thirteen neurons constitute a group of *escape response neurons* containing sensory neurons responsible for modulating escape reflex reactions upon different stimuli, as described below [37]

Neuron(s)	Noxious factor
FLPL/R	Harsh touch, low temperature (head)
PHBL/R	Chemicals
PHCR	High temperature (head)
PLMR	Gentle touch (tail)
PQR	CO ₂
PVDL/R	Harsh touch, low temperature
SDQL	High O ₂
SAAVL/R	no known factor
VD11	no known factor

D. Information propagation in the connectome: biological input scenarios

Despite the modest size of its nervous system, *C. elegans* can sense a range of mechanical, chemical and thermal factors [37]. Although it is believed that a stimulus results in motor action due to information flow progressing roughly from sensory neurons through interneurons to motor neurons [41], the underlying mechanisms and signal flows are still far from understood. In the absence of detailed measurements that can probe such pathways, we use here a simple diffusive dynamics as a rough approximation to more realistic nonlinear dynamical models, in order to mimic the signal propagation in this directed network. Such an approach, already suggested by Varshney et al. [4], is naturally linked to the multiscale community detection performed through Markov Stability and to the identification of flow roles through Role Based Similarity. Indeed, both methods used here (MS and RBS) are intrinsically defined in terms of a linear, diffusive process on the graph. In this section, we mimic the propagation of external stimuli applied at neurons that have been associated to particular biological inputs in the literature, and examine this dynamics in terms of the flow roles obtained above. More specifically, we choose a normalised initial condition $\phi(0)$ purely localised on a set of neurons and observe its decay towards the stationary solution π (see Eq. (4) in Section IV B). The approach to stationarity on every node is governed by:

$$\theta(t) = \phi(t) - \pi, \quad (1)$$

where $\theta(t)$ is the vector describing the amount of flow present at each node at time t , and π is the stationary state. Initially, $\theta_i(0)$ is positive only for those neurons where we inject the signal and negative for all other neurons. Eventually, $\phi(t)$ converges to π , and all the components of $\theta(t) \rightarrow 0$. Note that $\theta_i(t)$ only becomes positive if neuron i receives an influx of flow that drives it to ‘overshoot’ above its stationary value. Neurons can also approach stationarity monotonically without overshoot-

ing, depending on the particular input and the relative location of the neuron.

We have conducted four case studies in which we localised our inputs on specific groups of sensory neurons associated to biological scenarios:

- (i1) posterior mechanosensory stimulus [5, 7]:
PLML/R, PVDL/R, PDEL/R,
- (i2) anterior mechanosensory stimulus [5, 7]:
ADEL/R, ALML/R, AQR, AVM, BDUR/L,
FLPL/R, SIADL/R,
- (i3) posterior chemosensory (anus mechanosensory) stimulus [7, 42]:
PHAL/R, PHB/R
- (i4) anterior chemosensory stimulus [42]:
ADLL/R, ASHL/R, ASKL/R.

We concentrate here on the propagation of the posterior mechanosensory stimulus (i1). The detailed results for the other stimuli can be found in the *SI*. As shown in Figure 7a, the flow signal progresses in the expected ‘downstream information processing’ following the input of stimulus (i1). At first, the signal is concentrated on the input neurons (mostly sensory). With evolving time, the signal propagates out and the sensory neurons decay towards stationarity. From the inputs, the signal is in fact forwarded primarily to interneurons, as can be seen by the increase of the average value of θ for this class, peaking at $t \approx 1.5$. In turn, the signal is passed on from the interneurons to motor neurons, leading to a decay of θ towards stationarity for the interneurons whereas the motor neurons increase towards their stationary value. The input at the sensory neurons gets routed through the interneurons to the motor neurons, in a progression consistent with the expected biological processing. Although, this characteristic is observed in all scenarios (i1)-(i4), specific pathways of signal flow are different in all cases.

To detect important neurons, we select those units with large overshoots relative to their stationary value: $\max_t \theta(t)_i / \pi_i > 2/3$, i.e., those receiving the strongest influx of flow. According to this criterion, we obtain 26 neurons for scenario (i1), in addition to the 6 input neurons PLML/R, PVDL/R, PDEL/R, and we record their peak time to get an estimate of the time when they are most active. Fig. 7c shows that the peak times occur in two time windows (in addition to the input neurons, which peak at the beginning). In a first wave of activation peaks around $t \approx 1$ (see Fig. 7d), mainly interneurons overshoot over their stationary value, including those responsible for mechanosensory integration such as AVDL/R, DVA and the forward motion drivers PVCL/R [5, 37]. The second wave of activation peaks at around $t \approx 3$ contains predominantly ventral B-type motor neurons: DB2-7, VB11. B-type motor neurons are responsible for forward motion, a plausible biological response for a posterior mechanosensory stimulus [7, 37].

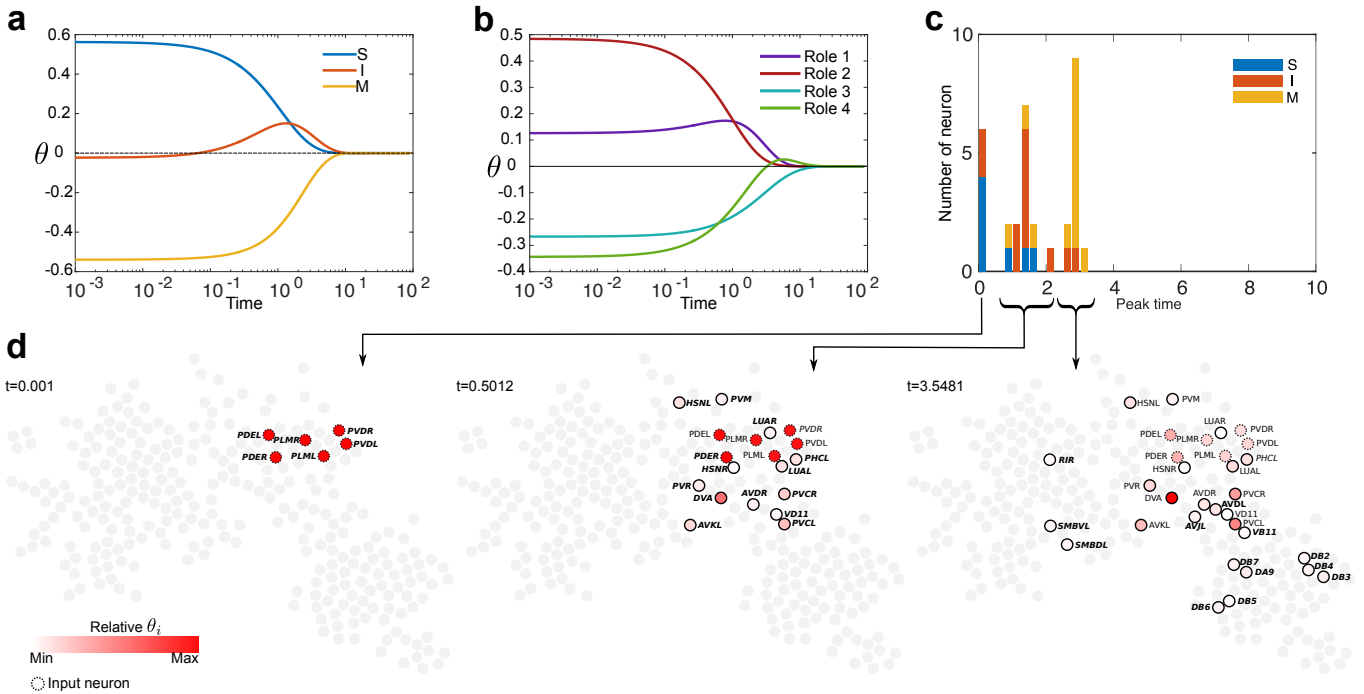


Figure 7. **Signal propagation: posterior mechanosensory stimulus.** Signal propagation governed by (4) from an initial condition localised at mechanosensory neurons (i1). (a) The approach to stationarity ($\theta(t) \rightarrow 0$) indicates that the input goes from sensory to motor neurons through an intermediate time where interneurons overshoot. (b) The stimulus (i1) is highly localised on R2 neurons and induces an overshoot of R4 neurons. (c) The propagation induces a cascade of overshooting neurons with large peaks: 32 neurons have peaks such that $\max_t \theta_i(t)/\pi_i > 2/3$ and the time of their peaks occurs in two bursts. Note the overall trend from S to I to M during the signal propagation. (d) The 32 overshooting neurons in (c) on the network to summarise the stages of signal propagation.

Interestingly, in cases (i2)-(i4), we observe equal excitation of A- and B-type motor neurons. In addition, a substantial excitation of motor neurons (in a protacted second wave of activation peaks) is only observed for posteriorly located stimuli (i1) and (i3). Further information and comparisons can be found in the *SI*.

These patterns of propagation can be linked to the observation that for (i1) and (i3), the majority of inputs is localised on the *escaping response group* R2. This is consistent with R2 corresponding to posterior upstream units. Specifically, for stimulus (i1) we observe that with evolving time the signal flows quickly from R2 towards the other upstream group R1, followed by propagation towards the downstream group R4 (see Fig. 7b). This progression mirrors the strong connections of the R2 group with motor neurons in R1 (AVDL/R and DVA) and R4 (PVCL/R), as discussed above. Finally, the signal spreads to R3, the head-centric downstream unit. Although very simplified, this simple signal propagation simulation can provide valuable insights into the directions of information flow in the connectome from sensory neurons through interneurons to motor neurons. Furthermore it sheds light on the meaning of roles R1-R4, indicating that indeed information flows very fast from R2 to motor neurons, as could be expected from neurons triggering an escape response.

III. DISCUSSION

We have presented an integrated analysis of the connectome of *C. elegans* in terms of directed flows from a network-theoretic perspective. Although the diffusive process used here is only a coarse approximation of physiological signal propagation, it can still be used to extract systemic features of the connectome, and to aid in the identification of promising candidates for experimental evaluations, as suggested by Varshney et al [4]. Here, we have exploit the connection between diffusive processes and graph-theoretical properties, which intimately links structure and dynamics, to elucidate relevant features in the *C. elegans* connectome with possible functional implications. We have used this perspective to analyse the connectome from two different viewpoints.

Firstly, using the diffusion-based Markov Stability framework, we have detected modules based on (directed) signal flow at different resolutions. We find 5 partitions at different granularity, from the finest partition, which separates neurons into groups corresponding to anatomical classes (S,I,M neurons) and location along the body of the worm, to the coarsest (bi)partition, which segregates the connectome into an S/I-dominated and M-dominated groupings. Remarkably, the partitions found are in good accordance with current knowledge of *C. elegans* physi-

ology, and provide insight into candidate neurons for further experimental investigations, e.g., the special role of the AVF and AVH neurons found in our analysis. Previous studies [20–22] aiming at uncovering modules in the *C. elegans* connectome have approached this issue from a structural point of view, neglecting possible dynamical implications and imposing an intrinsic scale so as to find just one partition. In contrast, the Markov Stability framework scans across all scales by sweeping through Markov time [26] in order to reveal the intrinsic, quasi-hierarchical organisation of the connectome, and through this link with diffusive processes it further gives insight into relevant features of signal propagation in the connectome. In the *SI* we provide a detailed comparison of the MS multiscale community structure with the partitions obtained using Modularity [20, 21], stochastic block models [22] and the MapEquation package [43].

Secondly, using the Role-Based-Similarity framework, we shed light on the functional structure of the *C. elegans* nervous system in terms of the *roles* the neurons play with respect to flow dynamics. RBS revealed two groups of upstream neurons and two groups of downstream neurons, with a specific inter-connectivity pattern that is reflected in the propagation of input signals motivated by particular biological scenarios. In particular, we find a small group of upstream neurons (R2) which are related strongly to posterior stimuli and motor reflexes and have been functionally linked to escape responses from noxious stimuli. Previous studies have assigned roles to neurons following the classification proposed by Guimera et al [44] or by exploring the core-periphery structure [45]. In contrast, the RBS method used here classifies nodes according to features of incoming and outgoing flow patterns at all scales. This more nuanced use of the flow information in the network enables us to go beyond a classification based on immediate neighbourhoods only, or combinatorial classifications such as regular and structural equivalence [27, 30]. (See the *SI* for a comparison of RBS roles and those obtained through regular equivalence [46].) Such classification reveals a graded organisation of the nodes in terms of upstream-downstream information distribution, which is again linked to signal propagation.

Finally, our dynamical approach naturally allows for a systematic study the effect of single and double neuron ablations, in terms of how they disrupt the signaling flow in the network and thus the detected flow-based partitions. Similarly, it enabled us to conduct simple ‘input-response’ experiment, which have revealed the relevance of the detected flow roles for signal propagation. These computational studies can aid in the design of experimental studies leading towards the integration of information at the system level, with the eventual aim of linking wiring properties of the connectome with information processing and functional behaviour.

IV. MATERIALS & METHODS

A. The *C. elegans* neuronal network

We encode the biological information of the connectome into an $N \times N$ adjacency matrix ($N = 279$) denoted by A , where each entry $A_{ij} \in \mathbb{N}$ counts the total number of synapses, including both chemical synapses and gap junctions, connecting neuron i to neuron j . Chemical synapses are not necessarily reciprocal, hence $A \neq A^T$. In other words, the connectome is a *directed, weighted network*. The network is relatively sparse, with 2990 edges: 796 of the edges are formed by gap junctions only; 1962 contain only chemical synapses; whereas in 232 edges both electrical and chemical synapses are present. The vector of out-strengths, which compiles the sum of all different synapses per neuron, is $\mathbf{d} = A\mathbf{1}$. The average out-strength per neuron is ~ 29 , with a maximum of 256 attained by neuron AVAL, whereas the motor neuron DD6 is the only sink in the network, i.e., it has no outgoing connections. Note that although weakly connected, this directed network is *not* strongly connected.

B. Propagation dynamics in the network

Methods with different levels of complexity have been used to study signal propagation in the *C. elegans* connectome (see, e.g., Refs. [4, 41, 47–49]). Here, we use a continuous-time diffusion process as a simple proxy for the spread of information in this neuronal networks. Note that gap junctions may be simply modelled as a linear resistor and, although chemical synapses are likely to introduce nonlinearities, their sigmoidal transmission functions maybe linearised around an operating point to give an approximate linear model. Although simplified, such linear models have been successfully applied for the analysis of the spatio-temporal behaviour of strongly nonlinear neuronal networks [50, 51]. More specifically, as remarked by Varshney et al. [4], such an approach has additional merit in *C. elegans*, where neurons do not fire classical action potentials and have chemical synapses that likely release neurotransmitters tonically [52]. Thus, linear systems analysis can provide interesting insights in this system [4].

In this model, the signal on the nodes at time t is represented by the $1 \times N$ row vector $\phi(t)$, which evolves under the following differential equation:

$$\frac{d\phi}{dt} = \phi[M - I], \quad (2)$$

where I is the identity matrix and M is the transition matrix defined as follows:

$$M = \tau D^\dagger A + \frac{1}{N} [(1 - \tau)\mathbf{1} + \tau \mathbf{1}_{d_i=0}] \mathbf{1}^T. \quad (3)$$

Here, $\tau \in (0, 1)$ is the Google teleportation parameter (we take $\tau = 0.85$ throughout as is customary in the

literature); $\mathbb{1}_{d_i=0}$ is the indicator vector of nodes with zero out-strength (i.e., its i th component is one if $d_i = 0$ and zero otherwise); and D^\dagger is the pseudo-inverse of the degree matrix, i.e., a diagonal matrix with the inverse degrees,

$$D^\dagger_{ii} = \begin{cases} 0 & \text{if } d_i = 0 \\ 1/d_i & \text{if } d_i \neq 0 \end{cases}$$

The matrix M describes a signal diffusion along the directed edges with an additional (re-)injection of external ‘environmental noise’: each node receives inputs from its neighbours (which transmit the flow according to the relative weight along their outgoing links with probability τ) and receives a constant external re-injection of size $(1 - \tau)/N$. (For sinks, the outgoing flow is uniformly redistributed to all nodes, so as to avoid the signal accumulating at nodes with no out-links.) Mathematically, this (re-)injection of probability (known as teleportation in the networks literature) guarantees the existence of a unique stationary solution for Eq. (2), even when the network is not strongly connected [25, 53]. Biophysically, the teleportation can be understood as modelling the interactions with the random external environment.

Let $\phi(0)$ be the initial signal over the nodes at $t = 0$. Then the solution of Eq. (2) is:

$$\phi(t) = \phi(0) \exp(t[M - I]). \quad (4)$$

The stationary solution of this system is determined by π , the dominant left eigenvector of the matrix $\exp(t[M - I])$, which is given by $\phi(t \rightarrow \infty) = \phi(0)\mathbf{1}\pi$. If we choose a normalized input ($\phi(0)\mathbf{1} = 1$), the stationary solution is just the dominant left eigenvector π , also known as PageRank [53].

C. A dynamical perspective for community detection in graphs: Markov Stability

The diffusive dynamics defined by Eq. (2) can be exploited to reveal the multiscale structural organisation of the *C. elegans* connectome using the Markov Stability community detection framework [23–25].

Markov Stability operates by optimising a cost function parametrically dependent on time (to be defined below) over the space of all partitions. More formally, a partition \mathcal{P} of the N nodes of the network into C non-overlapping communities is encoded as a $N \times C$ indicator matrix H , such that

$$H_{ic} = \begin{cases} 1 & \text{if node } i \text{ belongs to community } c \\ 0 & \text{otherwise.} \end{cases} \quad (5)$$

Given the partition matrix H , we define the time-dependent *clustered autocovariance matrix*:

$$R(t, H) = H^T [\Pi \exp(t[M - I]) - \pi\pi^T] H, \quad (6)$$

where $\Pi = \text{diag}(\pi)$ contains the stationary distribution on the diagonal. The kl -th entry of $R_{kl}(t, H)$ quantifies how likely it is that in a diffusion process of duration t a random walker that starts in community k ends in community l , minus the probability for such an event to happen by chance. To find groups of nodes where flows are trapped more strongly over time t than one would expect at random, we must find a partition \mathcal{P} (and accordingly its matrix $H_{\mathcal{P}}$) for which

$$r(t, H_{\mathcal{P}}) = \text{trace } R(t, H_{\mathcal{P}}) \quad (7)$$

is maximal. We call $r(t, H_{\mathcal{P}})$ the *Markov Stability* of the partition \mathcal{P} at time t [23, 25].

To obtain the relevant community structure with respect to the diffusion process, we maximise $r(t, H)$ in the space of all partitions for each time t . This results in a time-dependent sequence of optimal partitions:

$$\mathcal{P}_{\max}(t) = \arg \max_{\mathcal{P}} r(t, H_{\mathcal{P}}). \quad (8)$$

Although the optimization problem (8) is NP-hard, there are efficient heuristic algorithmic optimisations that work well in practice. In particular, it has been shown that this optimisation can be carried out using any algorithm devised for modularity maximisation [23–25].

In this work, we use the Louvain algorithm [54], which is known to offer high quality solutions for this NP-hard problem whilst remaining computationally efficient.

To get a good estimate of $\mathcal{P}_{\max}(t)$, the Louvain optimisation is run $\ell = 100$ times with different random initialisations for each time t . This computation results in an ensemble of solutions for each of the Markov times, $\{\mathcal{P}_i(t)\}_{i=1}^{\ell}$. From this set of partitions we pick the best partition $\hat{\mathcal{P}}(t)$ for each time t according to our measure (7). Ideally, the optimised partitions we pick at each time will be a close estimate of the true optimum:

$$\hat{\mathcal{P}}(t) \approx \mathcal{P}_{\max}(t).$$

To identify important partitions and time scales, we use two robustness criteria [26, 55]:

Consistency of the optimised partition: A relevant partition should be associated with a robust outcome of the optimisation. To assess the consistency of the optimisation, we compute the average *normalised variation of information* [56], over the ensemble of Louvain solutions:

$$\langle VI(t) \rangle = \frac{1}{\ell(\ell - 1)} \sum_{i \neq j} VI(\mathcal{P}_i(t), \mathcal{P}_j(t)) \quad (9)$$

where the variation of information between two partitions \mathcal{P} and \mathcal{P}' is defined as [56]:

$$VI(\mathcal{P}, \mathcal{P}') = 2H(\mathcal{P}, \mathcal{P}') - H(\mathcal{P}) - H(\mathcal{P}'). \quad (10)$$

Here $H(\mathcal{P}) = -\sum_C p(\mathcal{C}) \log p(\mathcal{C})$ is a Shannon entropy, with $p(\mathcal{C})$ giving the relative frequency of finding a node

in community \mathcal{C} in partition \mathcal{P} . $H(\mathcal{P}, \mathcal{P}')$ is the Shannon entropy of the joint probability.

The computed $\langle VI(t) \rangle$ gives an average information-theoretical distance between all partitions obtained from the ℓ Louvain runs for each time t , and is used here to quantify the robustness of the solution to the optimisation. If all runs of the optimisation at t return the same partition, then $\langle VI(t) \rangle = 0$, indicating robustness of the partition to the optimisation. In general, low values of $\langle VI(t) \rangle$ indicate a robust partition; hence we select partitions with low values (or dips) of $\langle VI(t) \rangle$.

Persistence of the partition over time: Relevant partitions should also be optimal across stretches of Markov time. Such persistence is indicated by a plateau in the number of communities over time and by a low value plateau of the cross-time variation of information

$$VI(t, t') = VI(\widehat{\mathcal{P}}(t), \widehat{\mathcal{P}}(t')). \quad (11)$$

D. Quantifying the disruption of community structure under node deletion

The global effect on the network of node deletions can be assessed computationally by quantifying the disruption the deletion induces on the partitions found with Markov Stability. To mimic *in silico* the ablation of neuron i , we remove the i -th row and column of the adjacency matrix A , and analyse the change induced in the Markov Stability community structure of the reduced $(N-1) \times (N-1)$ matrix $A_{[i]}$. Double ablations are mimicked similarly, by simultaneously removing two rows (and the corresponding columns) from A to obtain the reduced $(N-2) \times (N-2)$ matrix $A_{[i,j]}$.

1. Detecting salient single-node deletions

We carry out a systematic study of all single node deletions in the network. To detect relevant single node deletions, we monitor either an induced loss of robustness or an induced disruption in the make-up of particular partitions, as follows.

Changes induced in the robustness of partitions: To detect which single-node deletions induce loss of robustness in each partition, we first run the MS analysis on *all* node deletions to obtain the sequence of optimised partitions and their intrinsic robustness across all times t :

$$\left\{ \widehat{\mathcal{P}}_{[i]}(t), \langle VI_{[i]}(t) \rangle \right\} \quad i = 1, \dots, N.$$

We then fit a Gaussian Process (GP) [57] to the ensemble of N time series $\{\langle VI_{[i]}(t) \rangle\}_{i=1}^N$, as well as the original, unablated $\langle VI(t) \rangle$. The resulting GP, with mean $\mu(t)$ and variance $\sigma^2(t)$, describes the average robustness of partitions under a single-node deletion.

Node deletions that induce a large change in the robustness of a given partition are outliers in the GP. For a partition $\widehat{\mathcal{P}}(t)$ optimal over the interval $t \in [t_1, t_2]$, we select node deletions i for which $\langle VI_{[i]}(t) \rangle$ differs from $\mu(t)$ by at least two standard deviations $\sigma(t)$ and, additionally, that this difference is sustained for at least a continuous time fraction of length $\ln(\sqrt{t_2/t_1})$ [55]. This criterion identifies node deletions that disrupt the robustness of a given partition over its epoch.

Changes induced in the make-up of partitions: To detect if a node deletion i induces a disruption to partition $\widehat{\mathcal{P}}(t)$, we compute the *community variation* defined as:

$$CV_{[i]}(\widehat{\mathcal{P}}(t)) = \min_{\tau} VI(\widehat{\mathcal{P}}(t), \widehat{\mathcal{P}}_{[i]}(\tau)), \quad (12)$$

i.e., the variation of information between $\widehat{\mathcal{P}}(t)$ and the most similar among *all* optimal partitions of the ablated network $\widehat{\mathcal{P}}_{[i]}(t)$ (with the deleted node always assigned to its own community). All the node deletions i are then ranked according to (12) for each partition.

2. Detecting double-node deletions with large supra-additive effects

We search for two-node deletions whose effect is larger than the summed effect of the two corresponding single node deletions. To this end, we define the community variation for the double ablation of nodes i, j as:

$$CV_{[i,j]}(\widehat{\mathcal{P}}(t)) = \min_{\tau} VI(\widehat{\mathcal{P}}(t), \widehat{\mathcal{P}}_{[i,j]}(\tau)), \quad (13)$$

which we compare against the average of the individual ablations, as given in (12):

$$CV_{[i,j]}(\widehat{\mathcal{P}}(t)) = \frac{CV_{[i]}(\widehat{\mathcal{P}}(t)) + CV_{[j]}(\widehat{\mathcal{P}}(t))}{2}. \quad (14)$$

To find node pairs with supra-additive effect, we use Quantile Regression (QR) [58], a method widely used in econometrics, ecology, and medical statistics. In contrast to standard least squares regression, which focusses on estimating the conditional mean of the samples, QR provides a method to estimate conditional quantile functions. For a given partition $\widehat{\mathcal{P}}(t)$, we apply QR to fit quantiles for the regression of $CV_{[i,j]}(\widehat{\mathcal{P}}(t))$ against $CV_{[i,j]}(\widehat{\mathcal{P}}(t))$, using all 38781 two-node ablations in the network (Fig. 5). We then find the quantiles above which 1% of the double deletions lie, and use this as our criterion to select double-ablations that have a strong effect. All scores are computed using Bayesian Quantile Regression, as implemented in the R package `BSquare` (<https://cran.r-project.org/web/packages/BSquare/index.html>), which fits all quantiles simultaneously resulting in a more coherent estimate [59–61]. Following Ref. [61], we fit the quantile to the normalised version of (14) using a gamma centering distribution and 4 basis functions.

E. Finding flow roles in networks: Role-Based Similarity

In directed networks, not all nodes have the same role, e.g., nodes can be sinks, sources or hubs [40, 62]. Although in complex directed networks, roles may not be defined as simply, they still may be characterised by the contribution of each node to the diffusion of in- and out-flows in the network. Here we use a recently developed method (Role-Based Similarity, RBS) to uncover roles in directed networks based on the patterns of incoming and outgoing flows at all scales [28, 29]. The main idea underpinning RBS is that nodes with a similar in/out flow profile have a similar role, regardless of whether they are near or far apart in the network. The similarity score between two nodes is obtained from the weighted number of in- and out-paths of increasing lengths, beginning and ending at each node. We encode this information in the feature matrix X :

$$X = \begin{bmatrix} \mathbf{x}_1 \\ \vdots \\ \mathbf{x}_N \end{bmatrix} = \left[\overbrace{\dots (\beta A^T)^k \mathbf{1} \dots}^{\text{paths in}} \mid \overbrace{\dots (\beta A)^k \mathbf{1} \dots}^{\text{paths out}} \right], \quad (15)$$

where $\beta = \alpha/\lambda_1$ with $\alpha \in (0, 1)$ and λ_1 is the spectral radius of the adjacency matrix A . The cosine similarity of their feature vectors gives the similarity between two nodes:

$$Y_{ij} = \frac{\mathbf{x}_i \mathbf{x}_j^T}{\|\mathbf{x}_i\|_2 \|\mathbf{x}_j\|_2}. \quad (16)$$

The $N \times N$ symmetric matrix Y quantifies how similar the connectivity profiles between nodes are. For instance, if nodes i and j have identical connectivity (i.e., $\mathbf{x}_i = \mathbf{x}_j$) then $Y_{ij} = 1$. If, on the contrary, they have nothing in

common (e.g., if i is a source node with no incoming connections and j is a sink node with no outgoing connections), then their descriptor vectors would be orthogonal and $Y_{ij} = 0$.

As outlined in Refs. [28–30], we compute the *similarity matrix* Y iteratively with $\alpha = 0.95$, and then apply the RMST algorithm to obtain a *similarity graph*, in which only the important information of Y is retained. We then extract *flow roles* in a data-driven manner without imposing the number of roles *a priori*, by clustering this similarity graph using Markov stability (see Fig. S2 in the SI). The low roles so obtained have been shown to capture [27, 30] relevant features of flow distribution in complex networks, where other measures of role classification based on combinatorial concepts and immediate neighbourhoods fail. In particular, our *flow roles* are fundamentally different from notions of roles used in social networks based on Structural Equivalence (SE) [39], and Regular Equivalence (RE) [40]. Because RE and SE do not incorporate information about the long scales of the network, they are unsuitable for complex networks such as the *C. elegans* connectome [27] (see Supplementary Data 2 and Figure S3 in SI for RE roles [46]).

Acknowledgements

KAB acknowledges support from the Imperial College Undergraduate Research Opportunities Programme (UROP) Award. MTS acknowledges support from the ARC and the Belgium network DYSCO (Dynamical Systems, Control and Optimisation). YNB acknowledges support from the G. Harold and Leila Y. Mathers Foundation. MBD acknowledges support from the James S. McDonnell Foundation Postdoctoral Program in Complexity Science/Complex Systems Fellowship Award (#220020349-CS/PD Fellow). MB acknowledges support from EPSRC grant EP/I017267/1 under the Mathematics Underpinning the Digital Economy program.

-
- [1] D. E. Donald, *C. elegans II* (Cold Spring Harbor Laboratory Press, 1997).
 - [2] J. G. White, E. Southgate, J. N. Thomson, and S. Brenner, Philosophical Transactions of the Royal Society of London. Series B, Biological Sciences **314**, 1 (1986).
 - [3] D. H. Hall and R. Russell, The Journal of neuroscience **11**, 1 (1991).
 - [4] L. R. Varshney, B. L. Chen, E. Paniagua, D. H. Hall, and D. B. Chklovskii, PLoS Computational Biology **7** (2011).
 - [5] M. Chalfie, J. E. Sulston, J. G. White, E. Southgate, J. N. Thomson, and S. Brenner, The Journal of Neuroscience **5**, 956 (1985).
 - [6] T. Wakabayashi, I. Kitagawa, and R. Shingai, Neuroscience Research **50**, 103 (2004).
 - [7] W. Li, L. Kang, B. J. Piggott, Z. Feng, and X. Z. S. Xu, Nature communications **2**, 315 (2011).
 - [8] G. Nagel, M. Brauner, J. F. Liewald, N. Adeishvili, E. Bamberg, and A. G. A., Current Biology **15**, 2279 (2005).
 - [9] S. Ibsen, A. T. C. Schutt, S. Esener, and S. H. Chalasani, Nature Communications **6** (2015).
 - [10] G. J. Stephens, B. Johnson-Kerner, W. Bialek, and W. S. Ryu, PLoS Comput. Biol. **4**, e1000028 (2008).
 - [11] E. Yemini, T. Jucikas, L. J. Grundy, A. E. Brown, and W. R. Schafer, Nature methods **10**, 877 (2013).
 - [12] A. E. Brown, E. I. Yemini, L. J. Grundy, T. Jucikas, and W. R. Schafer, Proceedings of the National Academy of Sciences **110**, 791 (2013).
 - [13] B. L. Chen, D. H. Hall, and D. B. Chklovskii, Proceedings of the National Academy of Sciences of the United States of America **103**, 4723 (2006).
 - [14] D. J. Watts and S. H. Strogatz, Nature **393**, 440 (1998).
 - [15] A.-L. Barabási and R. Albert, Science **286**, 509 (1999).
 - [16] E. K. Towilson, P. E. Vertes, S. E. Ahnert, W. R. Schafer, and E. T. Bullmore, The Journal of Neuroscience **33**(15), 63806387 (2013).

- [17] J. S. Kim and M. Kaiser, *Phil. Trans. R. Soc. B* **369** (2014).
- [18] A. Majewska and R. Yuste, *J Theor Biol* **212**, 155 (2001).
- [19] A. Arenas, A. Fernández, and S. Gómez, in *Bio-Inspired Computing and Communication* (Springer, 2008) pp. 9–18.
- [20] R. K. Pan, N. Chatterjee, and S. Sinha, *PLOS ONE* **5** (2010).
- [21] Y. Sohn, M.-K. Choi, Y.-Y. Ahn, J. Lee, and J. Jeong, *PLoS Comput. Biol.* **7** (2011).
- [22] D. M. Pavlovic, P. E. Vertes, E. T. Bullmore, W. R. Schafer, and T. E. Nichols, *PLoS ONE* **9(7)** (2014).
- [23] J.-C. Delvenne, S. N. Yaliraki, and M. Barahona, *Proceedings of the National Academy of Sciences* **107**, 12755 (2010), arXiv:0812.1811.
- [24] J.-C. Delvenne, M. T. Schaub, S. N. Yaliraki, and M. Barahona, in *Dynamics On and Of Complex Networks, Volume 2, Modeling and Simulation in Science, Engineering and Technology*, edited by A. Mukherjee, M. Choudhury, F. Peruani, N. Ganguly, and B. Mitra (Springer New York, 2013) pp. 221–242, arXiv:1308.1605.
- [25] R. Lambiotte, J. Delvenne, and M. Barahona, *Network Science and Engineering, IEEE Transactions on* **1**, 76 (2014), see also arXiv:0812.1770.
- [26] M. T. Schaub, J.-C. Delvenne, S. N. Yaliraki, and M. Barahona, *PLoS ONE* **7**, e32210 (2012).
- [27] M. Beguerisse-Díaz, G. Garduño Hernández, B. Vangelov, S. N. Yaliraki, and M. Barahona, *J R Soc Interface* **11** (2014), 10.1098/rsif.2014.0940.
- [28] K. Cooper and M. Barahona, arXiv:1012.2726 (2010), arXiv:1012.2726 [physics.soc-ph].
- [29] K. Cooper, *Complex Networks: Dynamics and Similarity*, Ph.D. thesis, University of London (2010).
- [30] M. Beguerisse-Díaz, B. Vangelov, and M. Barahona, in *2013 IEEE Global Conference on Signal and Information Processing (GlobalSIP)* (2013) pp. 937–940.
- [31] Y. N. Billeh, M. T. Schaub, C. A. Anastassiou, M. Barahona, and C. Koch, *Journal of neuroscience methods* **236**, 92 (2014).
- [32] J. M. Gray, J. J. Hill, and C. I. Bargmann, *PNAS* **102**, 3184 (2005).
- [33] G. Haspel and M. J. ODonovan, *The Journal of Neuroscience* **31(41)**, 14611 (2011).
- [34] M. T. Schaub, J. Lehmann, S. N. Yaliraki, and M. Barahona, *Network Science* **2**, 66 (2014), arXiv:1303.6241.
- [35] L. A. Hardaker, E. Singer, R. Kerr, G. Zhou, and W. R. Schafer, *Journal of Neurobiology* **49**, 303 (2001).
- [36] B. J. Piggott, J. Liu, Z. Feng, S. A. Wescott, and X. S. Xu, *Cell* **147**, 922 (2006).
- [37] D. Hall, Z. Altun, and L. Herndon, “Worm Atlas,” (2015).
- [38] E. L. Ardiel and C. H. Rankin, *Current Biology* **25**, R405 (2015).
- [39] F. Lorrain and H. C. White, *The Journal of Mathematical Sociology* **1**, 49 (1971).
- [40] M. G. Everett and S. P. Borgatti, *The Journal of Mathematical Sociology* **19**, 29 (1994).
- [41] T. A. Jarrell, Y. Wang, A. E. Bloniarz, C. A. Brittin, M. Xu, J. N. Thomson, D. G. Albertson, D. H. Hall, and S. W. Emmons, *Science* **337**, 437 (2012).
- [42] M. Hilliard, C. I. Bargmann, and P. Bazzicalupo, *Current Biology* **12**, 730 (2002).
- [43] D. Edler and M. Rosvall, “The MapEquation software package, available online at <http://www.mapequation.org>,”.
- [44] R. Guimera and L. A. N. Amaral, *Nature* **433**, 895 (2005).
- [45] N. Chatterjee and S. Sinha, “Understanding the mind of a worm: hierarchical network structure underlying nervous system function in *C. elegans*,” in *Models of Brain and Mind - Physical, Computational and Psychological Approaches*, Progress in Brain Research, Vol. 168 (Elsevier, 2007) pp. 145–153.
- [46] S. P. Borgatti and M. G. Everett, *Social Networks* **15**, 361 (1993).
- [47] A. Zaslaver, I. Liani, O. Shtangel, S. Ginzburg, L. Yee, and P. W. Sternberg, *Proceedings of the National Academy of Sciences* **112**, 1185 (2015).
- [48] C. Koch, *Biophysics of Computation* (Oxford University Press, 1999).
- [49] T. C. Ferree and S. R. Lockery, *Journal of Computational Neuroscience* **6**, 263 (1999).
- [50] A. L.-K. . B. Doiron, *Nature Neuroscience* **15**, 1498?1505 (2012).
- [51] M. T. Schaub, Y. N. Billeh, C. A. Anastassiou, C. Koch, and M. Barahona, *PLoS Computational Biology* **11**, e1004196 (2015).
- [52] M. B. Goodman, D. H. Hall, L. Avery, and S. R. Lockery, *Neuron* **20**, 763 (1998).
- [53] L. Page, S. Brin, R. Motwani, and T. Winograd, *The PageRank Citation Ranking: Bringing Order to the Web.*, Technical Report 1999-66 (Stanford InfoLab, 1999) previous number = SIDL-WP-1999-0120.
- [54] V. D. Blondel, J.-L. Guillaume, R. Lambiotte, and E. Lefebvre, *Journal of Statistical Mechanics: Theory and Experiment* **2008**, P10008 (2008).
- [55] B. Amor, S. N. Yaliraki, R. Woscholski, and M. Barahona, *Mol. BioSyst.* **10**, 2247 (2014).
- [56] M. Meilä, *Journal of Multivariate Analysis* **98**, 873 (2007).
- [57] C. E. Rasmussen and C. K. I. Williams, *Gaussian Processes for Machine Learning (Adaptive Computation and Machine Learning)* (The MIT Press, 2005).
- [58] R. Koenker, *Quantile regression*, 38 (Cambridge university press, 2005).
- [59] B. J. Reich, M. Fuentes, and D. B. Dunson, *Journal of the American Statistical Association* **106** (2011).
- [60] B. J. Reich, *Journal of the Royal Statistical Society: Series C (Applied Statistics)* **61**, 535 (2012).
- [61] L. B. Smith and B. J. Reich, *BSquare: An R package for Bayesian simultaneous quantile regression*, Tech. Rep. (North Carolina State University, 2013).
- [62] J. M. Kleinberg, *J. ACM* **46**, 604 (1999).